

Communication

Surface Curvature Sensor Based on Intracavity Sensing of Fiber Ring Laser

Liang Yi ^{1,*}, Zhifei Xue ¹, Yiyun Ding ², Min Wang ², Zekang Guo ² and Jia Shi ² 

¹ Department of Instrumentation, Aero Engine Corporation of China Commercial Aircraft Engine Co., Ltd., Shanghai 201306, China

² Tianjin Key Laboratory of Optoelectronic Detection Technology and System, School of Electronic and Information Engineering, Tiangong University, Tianjin 300387, China

* Correspondence: liangyi2231@163.com

Abstract: The measurement of surface curvature is of great significance in aerospace, structural health monitoring, energy batteries, etc. In this paper, a fiber-optic surface curvature sensor, based on intracavity sensing of fiber ring laser (FRL), is experimentally demonstrated. A no-core fiber-based filter performs as the sensing head of the FRL sensor. The response between the curvature of the NCF and the output wavelength of the FRL was investigated. In the measurement of curvature, the sensor system showed a narrow 3-dB bandwidth of 0.08 nm, with a high signal-to-noise ratio of about 60 dB. The curvature sensitivities were measured as -0.348 nm/m^{-1} within 0.2 m^{-1} , and -3.185 nm/m^{-1} from 0.2 m^{-1} to 0.475 m^{-1} . The performance of the surface curvature sensor was characterized by parameters, including output stability, temperature cross-sensitivity, and detection limit.

Keywords: fiber optics sensors; curvature; laser



Citation: Yi, L.; Xue, Z.; Ding, Y.; Wang, M.; Guo, Z.; Shi, J. Surface Curvature Sensor Based on Intracavity Sensing of Fiber Ring Laser. *Photonics* **2022**, *9*, 781. <https://doi.org/10.3390/photonics9100781>

Received: 16 September 2022

Accepted: 12 October 2022

Published: 20 October 2022

Publisher's Note: MDPI stays neutral with regard to jurisdictional claims in published maps and institutional affiliations.



Copyright: © 2022 by the authors. Licensee MDPI, Basel, Switzerland. This article is an open access article distributed under the terms and conditions of the Creative Commons Attribution (CC BY) license (<https://creativecommons.org/licenses/by/4.0/>).

1. Introduction

Surface curvature sensors, based on an all-fiber structure, have been widely investigated, due to their significant applications in aerospace, structural health monitoring, energy batteries, etc. Compared with traditional electromagnetic sensors, the fiber-optic sensors have advantages of anti-interference, compact size, high sensitivity, and fast responses. Several fiber-optic surface curvature sensors with special structures have been demonstrated, such as the fiber gratings [1,2], cavity ring down configuration [3], Mach-Zehnder interferometers [4–7], multimode interferometers [8,9], and tapered fiber [10]. Multicore fibers have also been applied to measure curvature by probing the super-modes [11,12]. Arnaldo Junior and colleagues offer new opportunities to create fiber-optic curvature sensors based on polymer optical fibers [13–15] and they have developed important compensation techniques and applications [16–18]. Traditional fiber-optic sensors have a resonant wavelength for sensing with a wide spectral bandwidth. They are usually measured by a broadband light source and demodulated by an optical spectrum analyzer (OSA). However, the accurate determination of the resonant wavelength is limited to their wide spectral bandwidth [19].

Recently, intracavity sensors, based on the fiber ring laser (FRL), have attracted great attention, due to their excellent performance in narrowing the spectral bandwidth in communication windows for accurate measurement [20] and remote detections [21]. Different types of FRL sensors have been developed to measure bend [19], strain [20], refractive index (RI) [22], temperature [23], and gas concentration [24]. Some of them have temperature cross-sensitivity in measurement. Simultaneously, the sensing head developed in the FRL sensor, may bring output decline to the emission wavelength and intensity. As a consequence, the applications of the intracavity sensors are mainly limited by cross-sensitivity and output stability.

In this work, an intracavity curvature sensor, based on the FRL embedded with no-core fiber (NCF), is demonstrated. Multimode interference is induced in the laser cavity with the structure of single-mode–no-core–single-mode (SNCS) fiber, which works as the filter and sensing head in the system simultaneously. The response between the curvature of the NCF and the output wavelength of the FRL was experimentally investigated. What is more, the performance of the intracavity curvature sensor was characterized. The proposed sensor shows the advantages of low temperature cross-sensitivity, high output stability, and low detection limit.

2. Experimental Setup and Theory of Operation

The surface curvature sensor was fabricated by a short length of NCF embedded in an FRL. The structure of the sensor is illustrated in Figure 1.

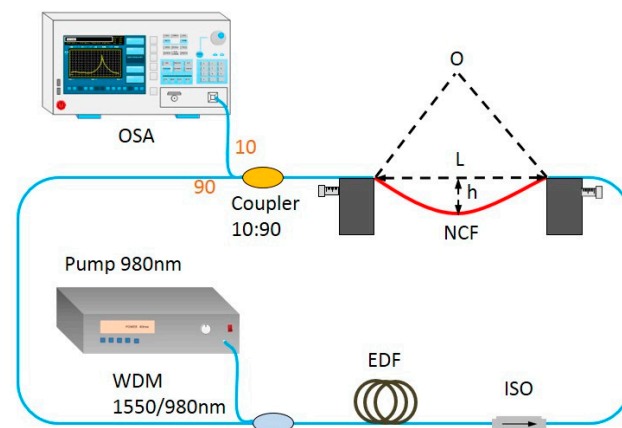


Figure 1. The structure of the surface curvature sensor.

Erbium-doped fiber (EDF, Nurfen, EDFC-980-HP), with a length of 3 m, was used as the gain medium of the FRL and was pumped by a 980-nm diode laser via a WDM coupler (980/1550 nm). An isolator (ISO) worked to force the laser oscillation to propagate in the clockwise direction. The coating of the NCF was removed with a diameter of 100 μm (Tianjin Opticontact Technology Development Co., Ltd., China). Then, the NCF was spliced between two single-mode fibers in the laser cavity, which formed the SNCS fiber. The SNCS fiber was located at the center of two clamps to experience different curvatures. As shown in Figure 1, the curvature can be calculated by:

$$k_{cur} = 8h / (4h^2 + L^2) \tag{1}$$

The output spectrum of the FRL was recorded by the OSA (YOKOGAWA, AQ6370) with a wavelength resolution of 0.02 nm. In the SNCS fiber, when the light was coupled from the single-mode fiber into the NCF, high order eigenmodes in the NCF were excited and multimode interference occurred in these modes. Assuming only the symmetric mode LP_{0m} had been excited in the NCF, then only linear polarized radial modes would be excited. With the field profile of LP_{0m} mode defined as $\psi_m(r)$, the input field of the SNCS fiber is:

$$E(r, 0) = \sum_{m=1}^M c_m \psi_m(r) \tag{2}$$

where r is the radial coordinate of the cross section in the NCF. For the LP_{0m} mode, c_m is the excited coefficient with the mode order of M , which is given by:

$$c_m = \frac{\int_0^\infty E(r, 0) \psi_m(r) r dr}{\int_0^\infty \psi_m(r) \psi_m(r) r dr} \tag{3}$$

The transmission field distribution of the light in the NCF can be written as:

$$E(r, z) = \sum_{m=1}^M c_m \psi_m(r) \exp(i\beta_m z) \tag{4}$$

where β_m is the propagating constant of the LP_{0m} and z is the distance. The difference of the longitudinal propagation constants between LP_{0m} mode and LP_{0n} mode is calculated as [25]:

$$\beta_m - \beta_n = \frac{u_m^2 - u_n^2}{2ka^2 n_{co}} \tag{5}$$

where $u_x = \pi(x - 1/4)$ with $x = m, n$ are the roots of the zeroth-order Bessel function. a and n_{co} are the radius and RI of the NCF, respectively. k is the free-space wavenumber. Then, the transmission spectrum of the SNCS fiber can be described as:

$$T(\lambda) = \sum_{m,n=1}^M c_m^2 c_n^2 \times \cos[(\beta_m - \beta_n)L] = \sum_{m,n=1}^M c_m^2 c_n^2 \times \cos\left(\frac{u_m^2 - u_n^2}{2ka^2 n_{co}} L\right) \tag{6}$$

where L is the length of the NCF. As the curvature of the NCF changes, the distribution of n_{co} along the NCF changes, which contributes to the changing of the transmission spectrum of the SNCS fiber. This process is schematically described in Figure 2 and the RI distribution can be expressed by [26]:

$$n_{co}(x, y) = n_{material} \left(1 + \frac{x}{R}\right) = n_{material} (1 + k_{cur} x) \tag{7}$$

where, $n_{material}$ is the RI of the bent waveguide cross-section. Thus, the curvature sensitivity can be obtained by the derivative of (6)

$$\frac{dT}{dk_{cur}} = \sum_{m,n=1}^M c_m^2 c_n^2 L \frac{u_m^2 - u_n^2}{2ka^2 n_{material}} \sin\left[\frac{u_m^2 - u_n^2}{2ka^2 n_{material} (1 + k_{cur} x)} L\right] \frac{k_{cur}}{(1 + k_{cur} x)^2} \tag{8}$$

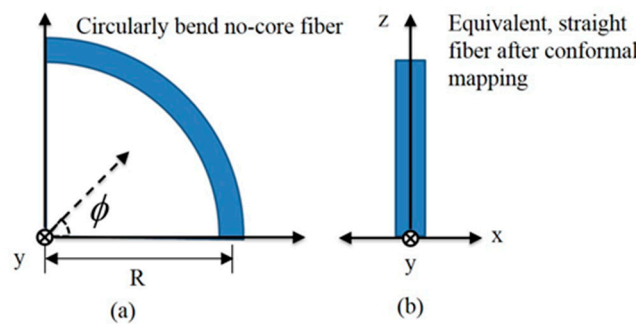


Figure 2. (a) Schematic diagram of the bent NCF and (b) the equivalent, straight NCF with conformal mapping. Light was guided along the ϕ and z directions, respectively.

From (8), it was proved that the curvature sensitivity of the sensor was nonlinear. The SNCS fiber performs as the filter and sensing head simultaneously in the proposed curvature sensor system. The emission wavelength of the FRL is at the minimum spectral transmission loss in the FRL system [21], which is mainly determined by the filtering characteristics of the sensing head. Therefore, as the curvature of the NCF varies, the output wavelength of the FRL changes, which can be used to measure the curvature.

3. Results and Discussion

When the curvature of the NCF was 0 m^{-1} , the transmission spectrum of the SNCS fiber was measured by a supercontinuum light source (NKT Photonics, SuperK COMPACT). When the pump power was set at 100 mW, the output spectrum of the FRL is shown in

Figure 3. The 3-dB bandwidth was obtained as ~ 0.08 nm with the signal-to-noise ratio (SNR) of ~ 60 dB. In the experiment, the 125-mm NCF was used to ensure a spectral overlap between the transmission peak of the SNCS fiber and the gain peak of the FRL. Simultaneously, the transmission spectrum of the SNCS fiber preferred to avoid multi-wavelength competition [27] which would make the output of the sensor unstable. Since the interference spectrum of the SNCS fiber was difficult to control in practice [28], many samples were fabricated and a suitable one was selected for the experiment.

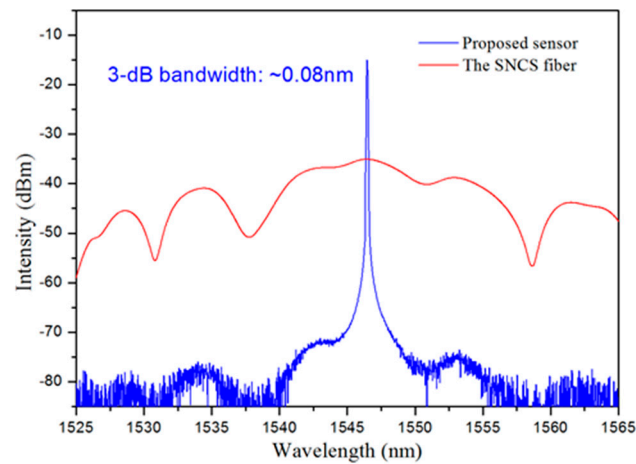


Figure 3. The spectrum of the sensing head and the FRL sensor system.

When the curvature of the NCF changed from 0 m^{-1} to 0.5 m^{-1} , the output spectra of the FRL sensor were measured, and are shown in Figure 4a.

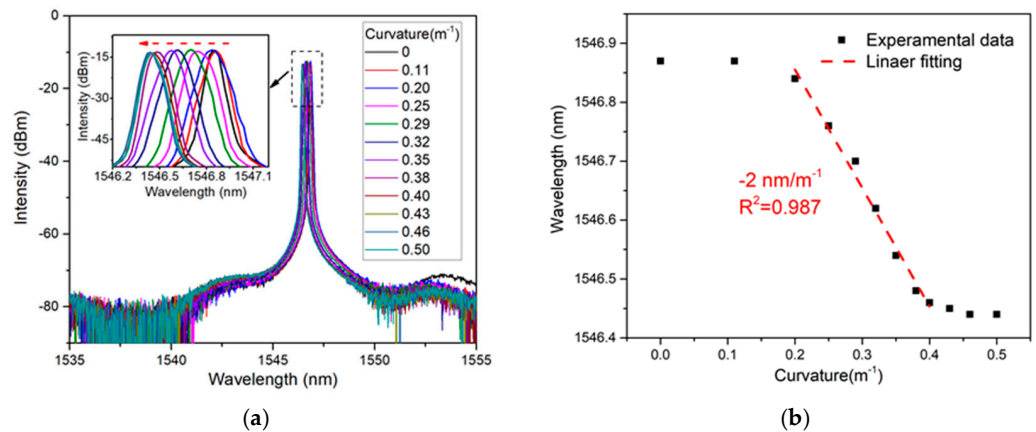


Figure 4. (a) The output spectra of the curvature sensor as the curvature of the NCF within 0.475 m^{-1} . (b) The curvature responses of the emission wavelength of the FRL sensor system and its linear fit.

As the curvature of the NCF changed from 0 m^{-1} to 0.5 m^{-1} , the emission wavelength of the fiber ring laser shifted from 1546.87 nm to 1546.44 nm . As shown in Figure 4b, there was a nonlinear response between the emission wavelength of the laser and the curvature of the NCF within 0.475 m^{-1} , which was similar to a passive curvature sensor, based on an SNCS fiber [29]. In order to evaluate the sensing ability of the sensor, the linear operations were applied to fit the curvature–wavelength curve with a range of 0 m^{-1} – 0.2 m^{-1} and 0.2 m^{-1} – 0.475 m^{-1} , respectively. The corresponding sensitivities were -0.348 nm/m^{-1} within 0.2 m^{-1} , and -3.185 nm/m^{-1} from 0.2 m^{-1} to 0.475 m^{-1} . In Figure 4b, when the curvature was more than 0.475 m^{-1} , the laser achieved the saturation of wavelength shift. That meant this sensor was mainly used in the low-curvature measurements from 0 m^{-1} to 0.475 m^{-1} .

The output stability of intracavity sensing in FRL sensors is important in practical applications. Therefore, the output stability of the curvature sensor system was measured.

In order to evaluate the stability of the sensor system, the output wavelength and intensity of the FRL sensor were monitored over 3 min by fixing the curvature at 0.202 m^{-1} and 0.351 m^{-1} , respectively. As shown in Figure 5, the wavelength perturbation was measured at less than 0.02 nm , which was limited by the OSA. The intensity perturbation was $\sim 0.6\text{ dBm}$. The result showed the sensor system had an excellent output performance in stability with little perturbation, due to the anti-interference ability of the SNCS fiber.

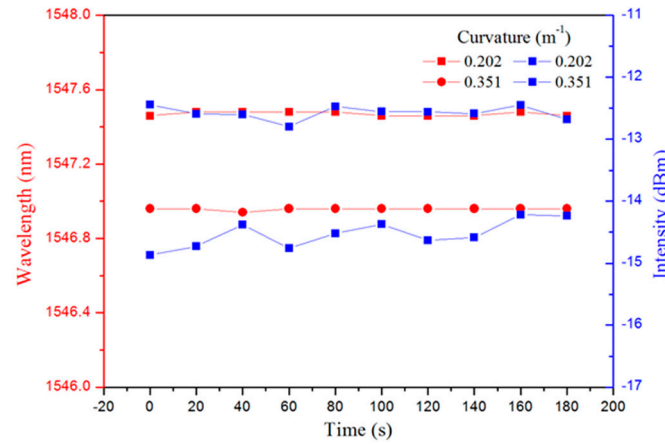


Figure 5. The output wavelength and intensity of the curvature sensor in 3 min by fixing the curvature at 0.202 m^{-1} and 0.351 m^{-1} , respectively.

In addition, the temperature cross-sensitivity of the curvature sensor was measured in a temperature chamber (VOS-30A, STIK CO. LTD, China) to experience temperature in a range from $20\text{ }^{\circ}\text{C}$ to $95\text{ }^{\circ}\text{C}$. The output spectra and the linear fit of the output wavelength are shown in Figure 6. As is depicted in Figure 6, as the temperature increased, the output wavelength of the curvature sensor had a small shift with the temperature sensitivity of $-3.3\text{ pm}/^{\circ}\text{C}$. The temperature stabilization with standard deviation was 0.088 nm . This indicated that the curvature sensor had a low sensitivity to temperature, which was much smaller than its sensitivity to curvature.

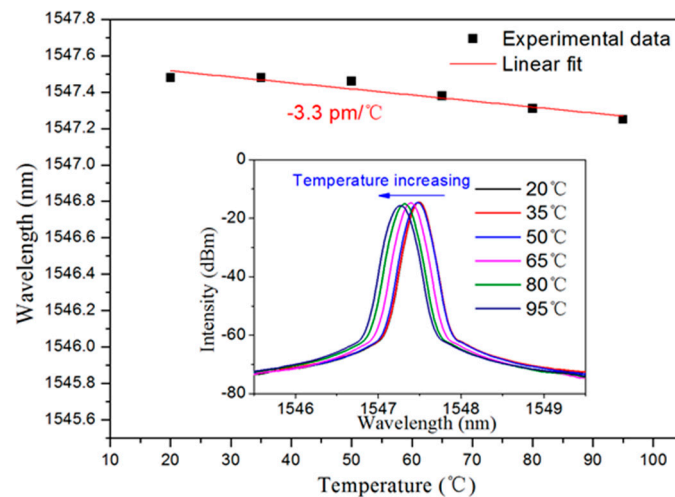


Figure 6. The linear fit of the output wavelength with the surrounding temperature increased from $20\text{ }^{\circ}\text{C}$ to $95\text{ }^{\circ}\text{C}$. Inset: the corresponding output spectra when the surrounding temperature increased.

The detection limit was used to analyze the performance of the curvature sensor, which took into account the sensitivity, spectral resolution of the system, and a number of noise parameters. The detection limit was calculated by R/S , in which R was the smallest detectable change for wavelength, which is called sensor resolution, and S was the

sensitivity of the device [30]. In this curvature sensor system, the resolution of the OSA was 0.02 nm. The 3-dB bandwidth was ~0.08 nm. The SNR was ~60 dB. The temperature stabilization with standard deviation was 0.088 nm from 20 °C to 95 °C. Thus, a low detection limit was obtained as 0.08 m⁻¹. Some similar fiber-optic curvature sensors are compared with this work in Table 1. The proposed sensor showed the advantages of low temperature cross-sensitivity and low detection limit.

Table 1. The performance of some similar fiber-optic curvature sensors.

Sensor	Highest Sensitivity (nm/m ⁻¹)	Temperature Cross-Sensitivity (pm/°C)	Detection Limit (m ⁻¹)	Ref.
Long-period fiber grating	30.85	76	N.A.	[31]
Microstructured fiber	1.118	>40	N.A.	[32]
In-fiber Mach–Zehnder interferometer	2.491	9.72	N.A.	[33]
Four-core fiber Mach–Zehnder interferometer	−18.75	74	0.042	[34]
SNCS fiber + FRL	−3.185	−3.3	0.08	This work

4. Conclusions

In this work, a surface curvature sensor system, based on intracavity sensing in an FRL, was demonstrated. A short length of NCF was inserted into the FRL, which formed the structure of the SNCS fiber. The SNCS fiber worked as the filter and sensing head in the curvature sensor system, simultaneously. As the curvature of the NCF varied, the filtering characteristics of the SNCS fiber changed, and, then, the output wavelength of the FRL shifted. The intracavity curvature sensor was obtained with a 3-dB bandwidth ~0.08 nm and SNR ~60 dB, and its curvature sensitivities were −0.348 nm/m⁻¹ within 0.2 m⁻¹, and −3.185 nm/m⁻¹ from 0.2 m⁻¹ to 0.475 m⁻¹. What is more, the performance of the curvature sensor was characterized by some parameters. The stability of the intracavity curvature sensor was measured by output wavelength and intensity in 3 min and the results showed that it had good stability. The temperature cross-sensitivity was also measured from 20 °C to 95 °C and it had a low temperature cross-sensitivity of −3.3 pm/°C. The detection limit was obtained as low as 0.08 m⁻¹. The proposed sensor shows the advantages of low temperature cross-sensitivity, high output stability, and low detection limit. It can be applied in aerospace, structural health monitoring, energy batteries, etc.

Author Contributions: Conceptualization, L.Y.; methodology, L.Y. and J.S.; software, L.Y.; validation, L.Y. and Z.G.; writing—original draft preparation, L.Y.; writing—review and editing, Z.X.; visualization, Y.D. and M.W.; supervision, L.Y. All authors have read and agreed to the published version of the manuscript.

Funding: This work is sponsored by the Natural Science Foundation of Tianjin City (19JCQNJC01400), the Open Research Fund of National Mobile Communications Research Laboratory, Southeast University (2022D12), and the Open Fund of IPOC, BUPT (IPOC2021B02).

Institutional Review Board Statement: Not applicable.

Informed Consent Statement: Not applicable.

Data Availability Statement: Not applicable.

Conflicts of Interest: The authors declare no conflict of interest.

References

1. Zhou, W.; Zhou, Y.; Dong, X.; Shao, L.Y.; Cheng, J.; Albert, J. Fiber-Optic Curvature Sensor Based on Cladding-Mode Bragg Grating Excited by Fiber Multimode Interferometer. *IEEE Photonics J.* **2012**, *4*, 1051–1057. [[CrossRef](#)]
2. Wu, Z.; Shum, P.P.; Shao, X.; Zhang, H.; Zhang, N.; Huang, T.; Humbert, G.; Auguste, J.L.; Gerome, F.; Blondy, J.M.; et al. Temperature- and strain-insensitive curvature sensor based on ring-core modes in dual-concentric-core fiber. *Opt. Lett.* **2016**, *41*, 380–383. [[CrossRef](#)] [[PubMed](#)]
3. Silva, S.; Biswas, P.; Bandyopadhyay, S.; Jorge, P.A.; Marques, M.B.; Frazao, O. Fiber-Optic Cavity Ring Down Using an Added-Signal for Curvature Sensing. *IEEE Photonics Technol. Lett.* **2015**, *27*, 2079–2082. [[CrossRef](#)]
4. Gong, H.; Xiong, M.; Qian, Z.; Zhao, C.-L.; Dong, X. Simultaneous Measurement of Curvature and Temperature Based on Mach-Zehnder Interferometer Comprising Core-Offset and Spherical-Shape Structures. *IEEE Photonics J.* **2016**, *8*, 1–9. [[CrossRef](#)]
5. Dass, S.; Jha, R. Micrometer Wire Assisted Inline Mach-Zehnder Interferometric Curvature Sensor. *IEEE Photonics Technol. Lett.* **2016**, *28*, 31–34. [[CrossRef](#)]
6. Zhang, Y.X.; Zhou, A.; Qin, B.Y.; Xu, Q.; Liu, Z.H.; Yang, J.; Yuan, L.B. Simultaneous Measurement of Temperature and Curvature Based on Hollow Annular Core Fiber. *IEEE Photonics Technol. Lett.* **2014**, *26*, 1128–1131. [[CrossRef](#)]
7. Fu, H.W.; Zhao, N.; Shao, M.; Li, H.D.; Gao, H.; Liu, Q.P.; Yong, Z.; Liu, Y.G.; Qiao, X.G. High-Sensitivity Mach-Zehnder Interferometric Curvature Fiber Sensor Based on Thin-Core Fiber. *IEEE Sens. J.* **2015**, *15*, 520–525.
8. Gong, Y.; Zhao, T.; Rao, Y.J.; Wu, Y. All-Fiber Curvature Sensor Based on Multimode Interference. *IEEE Photonics Technol. Lett.* **2011**, *23*, 679–681. [[CrossRef](#)]
9. Silva, S.; Pachon, E.G.P.; Franco, M.A.R.; Jorge, P.; Santos, J.L.; Malcata, F.X.; Cordeiro, C.M.B.; Frazao, O. Curvature and Temperature Discrimination Using Multimode Interference Fiber Optic Structures—A Proof of Concept. *J. Lightwave Technol.* **2012**, *30*, 3569–3575. [[CrossRef](#)]
10. Cano-Contreras, M.; Guzman-Chavez, A.D.; Mata-Chavez, R.I.; Vargas-Rodriguez, E.; Jauregui-Vazquez, D.; Claudio-Gonzalez, D.; Estudillo-Ayala, J.M.; Rojas-Laguna, R.; Huerta-Mascotte, E. All-Fiber Curvature Sensor Based on an Abrupt Tapered Fiber and a Fabry-Perot Interferometer. *IEEE Photonics Technol. Lett.* **2014**, *26*, 2213–2216. [[CrossRef](#)]
11. Van Newkirk, A.; Antonio-Lopez, J.E.; Velazquez-Benitez, A.; Albert, J.; Amezcua-Correa, R.; Schulzgen, A. Bending sensor combining multicore fiber with a mode-selective photonic lantern. *Opt. Lett.* **2015**, *40*, 5188–5191. [[CrossRef](#)] [[PubMed](#)]
12. Salceda-Delgado, G.; Van Newkirk, A.; Antonio-Lopez, J.E.; Martinez-Rios, A.; Schulzgen, A.; Correa, R.A. Compact fiber-optic curvature sensor based on super-mode interference in a seven-core fiber. *Opt. Lett.* **2015**, *40*, 1468–1471. [[CrossRef](#)]
13. Leal-Junior, A.G.; Frizzera, A.; Pontes, M.J. Analytical model for a polymer optical fiber under dynamic bending. *Opt. Laser Technol.* **2017**, *93*, 92–98. [[CrossRef](#)]
14. Leal-Junior, A.G.; Frizzera, A.; Pontes, M.J. Sensitive zone parameters and curvature radius evaluation for polymer optical fiber curvature sensors. *Opt. Laser Technol.* **2018**, *100*, 272–281. [[CrossRef](#)]
15. Leal-Junior, A.G.; Avellar, L.M.; Diaz, C.A.; Frizzera, A.; Marques, C.; Pontes, M.J. Fabry-Perot Curvature Sensor With Cavities Based on UV-Curable Resins: Design, Analysis, and Data Integration Approach. *IEEE Sens. J.* **2019**, *19*, 9798–9805. [[CrossRef](#)]
16. Leal-Junior, A.G.; Frizzera-Neto, A.; Pontes, M.J.; Botelho, T.R. Hysteresis compensation technique applied to polymer optical fiber curvature sensor for lower limb exoskeletons. *Meas. Sci. Technol.* **2017**, *28*, 125103. [[CrossRef](#)]
17. Leal-Junior, A.G.; Frizzera, A.; Marques, C.; Pontes, M.J. Viscoelastic features based compensation technique for polymer optical fiber curvature sensors. *Opt. Laser Technol.* **2018**, *105*, 35–40. [[CrossRef](#)]
18. Leal-Junior, A.G.; Frizzera, A.; Avellar, L.M.; Pontes, M.J. Design considerations, analysis, and application of a low-cost, fully portable, wearable polymer optical fiber curvature sensor. *Appl. Opt.* **2018**, *57*, 6927–6936. [[CrossRef](#)]
19. Xiong, H.; Xu, B.; Wang, D.N. Temperature Insensitive Optical Fiber Laser Bend Sensor With a Low Detection Limit. *IEEE Photonics Technol. Lett.* **2015**, *27*, 2599–2602. [[CrossRef](#)]
20. Bai, X.; Fan, D.; Wang, S.; Pu, S.; Zeng, X. Strain Sensor Based on Fiber Ring Cavity Laser With Photonic Crystal Fiber In-Line Mach-Zehnder Interferometer. *IEEE Photonics J.* **2014**, *6*, 1–8.
21. Shi, J.; Wang, Y.; Xu, D.; Su, G.; Zhang, H.; Feng, J.; Yan, C.; Fu, S.; Yao, J. Remote Magnetic Field Sensor Based on Intracavity Absorption of Evanescent Field. *IEEE Photonics J.* **2016**, *8*, 1–7. [[CrossRef](#)]
22. Liu, Z.B.; Tan, Z.W.; Yin, B.; Bai, Y.L.; Jian, S.S. Refractive index sensing characterization of a singlemode-claddingless-singlemode fiber structure based fiber ring cavity laser. *Opt. Express* **2014**, *22*, 5037–5042. [[CrossRef](#)] [[PubMed](#)]
23. Shi, J.; Wang, Y.Y.; Xu, D.G.; Zhang, H.W.; Su, G.H.; Duan, L.C.; Yan, C.; Yan, D.X.; Fu, S.J.; Yao, J.Q. Temperature Sensor Based on Fiber Ring Laser With Sagnac Loop. *IEEE Photonics Technol. Lett.* **2016**, *28*, 794–797. [[CrossRef](#)]
24. Zhang, H.W.; Lu, Y.; Duan, L.C.; Zhao, Z.Q.; Shi, W.; Yao, J.Q. Intracavity absorption multiplexed sensor network based on dense wavelength division multiplexing filter. *Opt. Express* **2014**, *22*, 24545–24550. [[CrossRef](#)] [[PubMed](#)]
25. Mohammed, W.S.; Mehta, A.; Johnson, E.G. Wavelength tunable fiber lens based on multimode interference. *J. Lightwave Technol.* **2004**, *22*, 469–477. [[CrossRef](#)]
26. Schermer, R.T.; Cole, J.H. Improved bend loss formula verified for optical fiber by simulation and experiment. *IEEE J. Quantum Electron.* **2007**, *43*, 899–909. [[CrossRef](#)]
27. Liu, Y.G.; Dong, X.Y.; Shum, P.; Yuan, S.Z.; Kai, G.Y.; Dong, X.Y. Stable room-temperature multi-wavelength lasing realization in ordinary erbium-doped fiber loop lasers. *Opt. Express* **2006**, *14*, 9293–9298. [[CrossRef](#)] [[PubMed](#)]

28. Hofmann, P.; Mafi, A.; Jollivet, C.; Tiess, T.; Peyghambarian, N.; Schulzgen, A. Detailed Investigation of Mode-Field Adapters Utilizing Multimode-Interference in Graded Index Fibers. *J. Lightwave Technol.* **2012**, *30*, 2289–2297. [[CrossRef](#)]
29. Ma, L.; Qi, Y.H.; Kang, Z.X.; Jian, S.S. All-Fiber Strain and Curvature Sensor Based on No-Core Fiber. *IEEE Sens. J.* **2014**, *14*, 1514–1517. [[CrossRef](#)]
30. White, I.M.; Fan, X.D. On the performance quantification of resonant refractive index sensors. *Opt. Express* **2008**, *16*, 1020–1028. [[CrossRef](#)] [[PubMed](#)]
31. Ma, Y.; Zhao, M.; Su, C.; Sun, J.; Li, X.; Yu, Z.; Zhang, L.; Geng, T. Vector curvature sensor based on asymmetrically polished long-period fiber grating. *Measurement* **2022**, *194*, 110997. [[CrossRef](#)]
32. Guo, Y.; Zhang, Y. A New Bamboo-Shaped Sensor for Curvature Measurement With Microstructured Fiber. *IEEE Photonics Technol. Lett.* **2021**, *33*, 619–622. [[CrossRef](#)]
33. Zhao, R.; Shu, X.; Xu, Z. Compact fiber curvature and temperature sensor inscribed by femtosecond laser through the coating. *J. Lightwave Technol.* **2021**, *39*, 3981–3990.
34. Xu, S.; Chen, H.; Feng, W. Fiber-optic curvature and temperature sensor based on the lateral-offset spliced SMF-FCF-SMF interference structure. *Opt. Laser Technol.* **2021**, *141*, 107174. [[CrossRef](#)]